Elsevier Editorial System(tm) for Nuclear Inst. and Methods in Physics Research, A
Manuscript Draft

Manuscript Number: NIMA-D-17-01100R1

Title: Position Resolution Simulations for the Inverted-coaxial Germanium Detector, SIGMA

Article Type: Full length article

Section/Category: Gamma, X-ray and Charged Particle Detectors

Keywords: Point contact germanium detector; γ-ray imaging; γ-ray tracking; Position sensitivity; Pulse shape analysis

Corresponding Author: Dr. Jonathan Paul Wright, Ph.D.

Corresponding Author's Institution: University of Liverpool

First Author: Jonathan Paul Wright, Ph.D.

Order of Authors: Jonathan Paul Wright, Ph.D.; Laura Harkness-Brennan; Andrew Boston; Daniel Judson; Marc Labiche; Paul Nolan; Robert Page; Fiona Pearce; David Radford; John Simpson; Carl Unsworth

Abstract: The SIGMA Germanium detector has the potential to revolutionise γ-ray spectroscopy, providing superior energy and position resolving capabilities compared with current large volume state-of-the-art Germanium detectors. The theoretical position resolution of the detector as a function of γ-ray interaction position has been studied using simulated detector signals. A study of the effects of RMS noise at various energies has been presented with the position resolution ranging from 0.33 mm FWHM at E_γ = 1 MeV, to 0.41 mm at E_γ = 150 keV. An additional investigation into the effects pulse alignment have on pulse shape analysis and in turn, position resolution has been performed. The theoretical performance of SIGMA operating in an experimental setting is presented for use as a standalone detector and as part of an ancillary system.

Position Resolution Simulations for the Inverted-coaxial Germanium Detector, SIGMA

J.P.Wright[a], L.J.Harkness-Brennan[a], A.J.Boston[a], D.S.Judson[a], M.Labiche[b], P.J.Nolan[a], R.D.Page[a], F.Pearce[a], D.C.Radford[c], J.Simpson[b], C.Unsworth[a]

[a]*University of Liverpool, Oliver Lodge Building, Liverpool, L69 7ZE, UK*
[b]*STFC, Daresbury Laboratory, Daresbury, Warrington, WA4 4AD, UK*
[c]*Physics Division, Oak Ridge National Laboratory, Oak Ridge, TN 37831, USA*

Abstract

The SIGMA Germanium detector has the potential to revolutionise γ-ray spectroscopy, providing superior energy and position resolving capabilities compared with current large volume state-of-the-art Germanium detectors. The theoretical position resolution of the detector as a function of γ-ray interaction position has been studied using simulated detector signals. A study of the effects of RMS noise at various energies has been presented with the position resolution ranging from 0.33 mm FWHM at $E_\gamma = 1$ MeV, to 0.41 mm at $E_\gamma = 150$ keV. An additional investigation into the effects pulse alignment have on pulse shape analysis and in turn, position resolution has been performed. The theoretical performance of SIGMA operating in an experimental setting is presented for use as a standalone detector and as part of an ancillary system.

Keywords: Point contact germanium detector, γ-ray imaging, γ-ray tracking, Position sensitivity, Pulse shape analysis

1. Introduction

The primary aim of the SIGMA (**S**egmented **I**nverted-coaxial **G**er**MA**nium) project is to demonstrate γ-ray tracking and imaging using point contact High Purity Germanium (HPGe) technology. SIGMA will be the first p-type segmented inverted-coaxial germanium detector to be manufactured. A similar large volume n-type HPGe detector utilising point contact technology was proposed in 2011 (1) with a working prototype currently being studied at Lawrence Berkeley National Laboratory (2).

One of the long term objectives is that detectors of this type could be deployed as part of the DEGAS HPGe array required for the DESPEC (DEcay SPECtroscopy) experiment (3) at FAIR (Facility for Anti-proton and Ion Research). Additionally, this detector would be ideally suited for use as a single detector γ-ray imaging device for commercial and industrial applications, enhancing performance in areas such as nuclear decommissioning, security, environmental monitoring and medical imaging.

One of the many benefits of using a point like contact is the reduced capacitance ($\sim$ 1 pF) of the electrode when compared to that of a standard coaxial detector ($\sim$10's of pF); a result of the reduced physical size of the contact. As a consequence, the signals from the point contact will exhibit extremely low series noise resulting in energy resolving capabilities superior to the current state-of-the-art large volume, segmented germanium detectors, an effect which is magnified at low energies. The energy resolution of a similar p-type Broad Energy Germanium (BeGe) detector was measured to be 0.5 keV at a γ-ray energy of 59.5 keV and 1.7 keV at an energy of 1332 keV (4).

The pulse shapes from the detector preamplifier are significantly altered from that of a standard coaxial detector due to the unique electrode configuration and inverted-coaxial design. The chosen configuration increases the charge collection time and creates a complex relationship between drift time and γ-ray interaction position. Using digitised charge pulses, in addition to pulse shape analysis (5) techniques, the interaction position is predicted to be localised to <1 mm^3 throughout the detector volume, up to 5 times better than obtained in current state-of-the-art large volume HPGe detectors such as AGATA (6) and GRETINA (7). This combination of energy and position resolution has the potential to improve the performance of γ-ray tracking and imaging algorithms which utilise the γ-ray interaction position and energy to kinematically reconstruct their paths.

2. Detector Design and Characterisation

The dimensions of the SIGMA crystal are illustrated in Figure 1, with the point contact being referred to as the rear of the detector. The crystal measures 70 mm maximum diameter by 80 mm length, with a taper reducing the radius of the crystal to 24.5 mm at the front face. The taper starts 20 mm from the rear of the crystal and tapers uniformly to the front face at an angle of 10^o. The core measures 10 mm in diameter and extends 55 mm into the bulk. The core, also known as a bore hole, enables large volume detectors to reach full depletion at a few thousand volts. The 6 mm diameter p^+ point contact is surrounded by a passivation region extending from $r = 3$ mm$\rightarrow r = 12$ mm as shown in blue in Figure 1.

The electrical segmentation scheme of the DC coupled outer contacts consists of 8 longitudinal rings, 2 concentric segments on the front face, 8

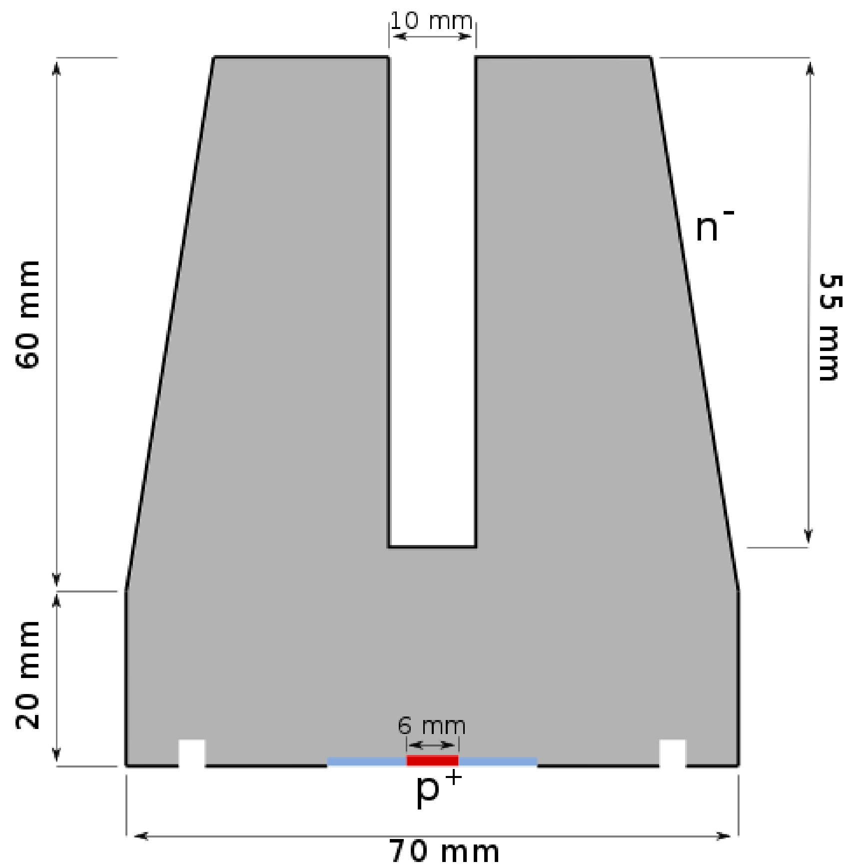

Figure 1: The SIGMA detector illustrating the dimensions of the crystal with the point contact shown in red (colour online).

azimuthal sectors, 1 core segment and a point contact on the rear face. Electrons will be collected by the 19 segments, with the holes being collected at the point contact. An illustration of the segmentation scheme is provided in Figure 2. The discussion will refer to a cylindrical coordinate system, (r, φ, z), where r is the radial distance from the central axis, φ is the angle around the central axis and z is the distance from the rear of the crystal perpendicular to r, with the centre of the point contact being $(r, z) = (0, 0)$. The angle

φ is defined with $\varphi = 0^o$ being the start of segment 1 and rotating around the segments in order. The 8 azimuthal segments provide angular information (φ), with the longitudinal rings used to resolve the depth of interactions (z). The addition of the front face segments and the core segments aid in resolving the radial position (r) of the γ-ray interaction. From hereon, the 8 azimuthal segments will be referred to as segments 1-8, with segments 9-16 being the 8 longitudinal rings. The 2 concentric rings on the front face make up segments 17 and 18, with segment 19 being the core segment. The detector is currently being manufactured by MIRION TECHNOLOGIES. The impurity profile of the crystal has been measured by the manufacturer to be 1.02×10^{10} cm^{-3} at the rear of the detector, with an impurity of 0.87×10^{10} cm^{-3} at the front face of the crystal. This results in an impurity gradient of -1.88×10^8 cm^{-4}, assuming a linear impurity gradient. The results presented are based on simulated work using these values and the physical dimensions described above.

2.1. Field Simulations

Simulations have been performed to calculate the electric and weighting potentials for SIGMA using a geometric adaptation of the FieldGen software developed at Oak Ridge National Laboratory (8). These simulations are crucial for calculating the drifts of charge carriers produced following a γ-ray interaction as they move through the crystal and measuring the expected response on each electrode. This software, along with the SigGen software (8), are established codes used for various experiments including GRETINA and MAJORANA. Simulations were initially performed to predict the voltage at which the detector fully depletes, with the results indicating full depletion

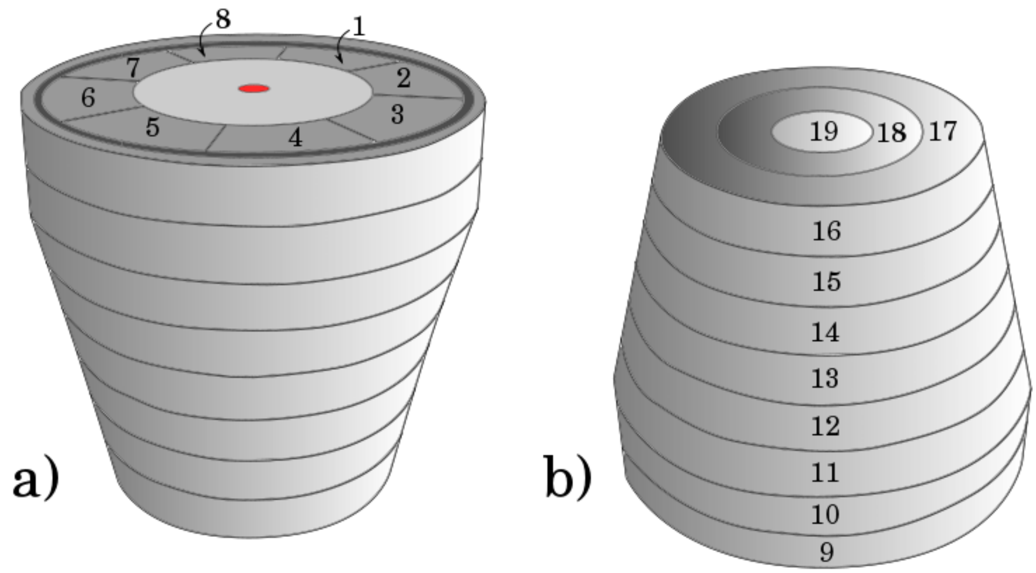

Figure 2: Schematic diagrams of the SIGMA detector showing the segmentation scheme with (a) and (b) showing the rear and front face of the crystal respectively. The point-like contact is coloured in red for illustrative purposes (colour online).

at -2000 V. Based on measurements made by the manufacturer, the recommended operational voltage was set at -3000 V. The electric potential and electric field strength for the SIGMA detector as a function of position have been calculated. Parameters included in the simulation were the operating voltage, detector geometry and electrode geometry. The results are shown for $\varphi = 0^o$ in Figure 3. The high voltage is applied directly to the point contact, with the outer DC coupled contacts being grounded. Figure 3a shows the short range of the electric potential, with the voltage reducing by $\sim$50% within 10 mm of the point contact. Figure 3b shows the electric field strength, which is the gradient of the electric potential at each point in the crystal. As can be seen, the field strength is very low for most of the detector, which when combined with long charge drift paths of the holes to the point contact, will result in very long drift times of up to 2μs.

The concept of a weighting potential (9; 10; 11) is used to calculate the instantaneously induced charge, Q, on an electrode, where

$$Q = q\Delta\varphi_0 \tag{1}$$

where q is the charge of the charge carriers and $\Delta\varphi_0$ is the change in the weighting potential. This enables theoretical detector signals to be produced. Therefore, the weighting potential has been calculated for the point contact, see Figure 4a and for each segment, examples of which are shown in Figure 6. Due to the rotational symmetry of the detector, only 1 weighting potential is calculated for the azimuthal segments on the rear of the detector. This potential is then used for all 8 segments.

2.2. Charge Transport Simulations

The SigGen (8) software has been used to track charge produced following a γ-ray interaction throughout the detector. Inputs to SigGen include the fields calculated by FieldGen, polarity, crystal temperature, detector impurity profile and the crystal lattice orientation. The electron drift velocity varies significantly as a function of temperature and crystallographic axis, with the crystallographic axis affecting the distance between atoms along the electric field lines changing for each orientation (12). In the simulation, charge is sampled as it drifts through the electric field at a frequency of 1 GHz, equating to a 1 ns sample size for the resulting charge pulses. For consistency, the 1 GHz pulses are downsampled to 100 MHz to match the sampling frequency that will be used by the digitiser cards for all experimental measurements, with each result comprising 200 samples.

The weighting potential is responsible for the shape of the charge pulses, with the point contact potential, Figure 4a, showing virtually zero potential throughout the detector followed by a large rise near to the contact. This short range potential is reflected in the resulting charge pulses, with a sharp rise in the pulse amplitude as the charge carriers near the point contact. Two example pulses are shown in Figure 4b, with the red and green circles in Figure 4a representing the γ-ray interaction positions corresponding to the red (solid) and green (dotted) pulses presented in 4b. This clearly demonstrates the temporal variation in the point contact pulse as a function of γ-ray interaction position. Due to this sharp rising edge, it is much easier to differentiate multiple interactions than in a comparable coaxial detector. Figure 5 shows all signals produced following a multi site event, with the point contact trace shown in red, the secondary collecting electrodes shown in green and the image charges highlighted blue. The point contact trace clearly shows 3 distinct rises followed by a plateau. This ability to distinguish multiple site events is one of the major advantages of a detector such as SIGMA over current large volume HPGe detectors. The difference in pulse quality can be seen in Figure 5 with comparative pulses for AGATA available in (13). By comparing the point contact signal to the secondary charge collecting electrodes, the reduced clarity is clear to see, with the larger physical size of the outer segments being more representative of the response seen in a standard coaxial detector. Figure 6 shows the weighting potentials for four example segments with the increased size of the electrode responsible for the increased spread in the weighting potential when compared with the point contact, Figure 4. This results in signals being induced on the contact at a much greater distance from the contact and explains the gradual slope in the charge pulses as opposed to the sharp rise seen in the point contact trace. The image charges (blue) shown in Figure 5 are a direct result of charge carriers passing through the weighting potentials of each electrode as they travel to their terminating electrode. This variation in the weighting potential causes a current to be induced on the electrode with the net charge returning to zero for non terminating electrodes.

2.3. Drift Time Distributions

Pulses provided by SigGen contain exact information regarding the starting time of the traces. The drift time as a function of position has been calculated as the time taken for the trace to rise from $0 \rightarrow 95\%$ of the pulse height. The drift time calculated as a function of (r, z) is presented in Figure 7a, with the top and bottom halves showing the distribution at $\varphi = 0^o$ and $\varphi = 45^o$ respectively. For this discussion, only the drift time measured on the point contact is considered.

This plot shows a very strong relationship between z position and drift time in the front of the detector, $\sim 25 < z < 80$ mm. In the rear of the crystal, the isochrone lines rotate and the direction of the gradient changes from longitudinal to radial. The variation between the two halves is due to the change in the crystallographic axis as a function of φ and can be seen more clearly in Figure 7b, which shows the variation in drift time as a function of φ for a γ-ray interaction at $(r, z) = (20, 20)$ mm. A clear oscillating behaviour is seen as the crystallographic axis varies as a function of φ, with a variation of $\sim$6% seen in the drift time.

To understand the drift paths of the electrons in this detector, the electron collecting electrode, outer hit segment, is plotted as a function of γ-ray interaction position in Figure 8. The relative sizes of each of the segments in Figure 8 are a direct result of the relative strengths of the weighting potentials shown in Figure 6 and provide a clearer image of the relative influence each electrode has on the charge collection path. The scale of the core contact is clear to see, with most interactions occurring near the central axis of the crystal terminating on the core. However for interactions occurring far from the central axis of the detector, there are clearly defined bands representing each of the outer contacts.

3. Position Sensitivity

The performance of tracking and imaging algorithms hinge on accurate measurement of γ-ray interaction energies and positions (14). With the excellent energy resolution of HPGe point contact detectors, the success of SIGMA as a tracking and imaging detector will depend on the position resolution attainable. To study this, simulated signals have been generated and processed through a grid search algorithm to reconstruct the initial γ-ray interaction position. The grid search algorithm utilises a simple χ^2 minimisation technique based on comparison between the charge pulses and a simulated pulse shape database; more detail is provided in section 3.1. A pulse shape database contains simulated charge pulses as a function of position for use in pulse shape analysis, with the database used in this work having a grid size of 1 mm x 3^o x 1 mm on a (r, φ, z) grid. As expected, the grid search algorithm perfectly reproduces the γ-ray interaction position when using the pulses directly generated from SigGen. In a laboratory environment, sources of noise and processing errors are introduced into the charge pulses. Examples of these effects, such as electronic noise and pulse alignment error, have been added to the simulation, with the effects of each on the final position resolution calculated.

3.1. Position Reconstruction

A grid search (GS) algorithm has been used to reconstruct the γ-ray interaction position. Tests were performed to study the most effective method of calculating the χ^2, in terms of both performance and time, where χ^2 was calculated as

$$\chi^2 = \sum_{i,j} |S^m_{i,j} - S^s_{i,j}|^2 \tag{2}$$

where $S^m_{i,j}$ and $S^s_{i,j}$ represent the modified and simulated pulses summed over the number of segments, i, and the number of samples, j. For the χ^2 study, three sets of search parameters, GS 1 $\rightarrow$ GS 3, were tested, with each set defined as

- GS 1 $\rightarrow$ Point contact + core + hit segment
- GS 2 $\rightarrow$ GS 1 + 8 $\times$ azimuthal segments
- GS 3 $\rightarrow$ All 19 segments + point contact

where the hit segment is defined as the electrode on which the electrons terminate. Since the size of the charge cloud in not accounted for in these simulations, there is no charge sharing and so there is only 1 hit segment for a single interaction. For the case when the electrons terminate on the core or one of the 8 azimuthal segments, the algorithm discards the 'hit segment' trace from the calculation to prevent double counting.

For the study, a simulated pulse is taken for a single position, with a random Gaussian noise added to each sample to simulate the electronic noise, defined by the root mean square (RMS). The χ^2 is then calculated against each pulse in the basis, with the lowest value of χ^2 taken as the most likely interaction position. The difference between the known interaction position and the measured position is then recorded. This process is repeated for each position in the detector on a 1 mm $\times$ 1 mm $\times$ 3^o grid. For this work to be valid, all knowledge of the input pulse must be unknown prior to the grid search. Since all of the effects added to the pulses are based on random distributions, this condition holds true and all post processing is done with no knowledge of the initial pulse.

To simulate the electronic noise, a random Gaussian distributed noise was added to each sample in the chosen pulse. Based on experimental measurements from a BEGe detector (4), the electronic noise was measured to be $\sim$1 mV peak-to-peak. For white noise, the relationship $V_{rms} = 6.6 \times V_{pp}$ holds true such that only 0.1% of the time, the RMS noise, V_{rms}, will exceed the nominal peak-to-peak value, V_{pp}, (15), giving a typical RMS noise of 0.15 mV for the point contact. When processed through a typical 100 mV/MeV charge sensitive preamplifier, the average noise is $\sim$1.5 keV which gives a normalised RMS noise of $\sim$1% when assuming a γ-decay of E_γ = 150 keV and 2% at 75 keV. For the study using normalised pulses, the value of 2% at

75 keV was used as the standard deviation to demonstrate the performance capabilities at low energies, with the mean centred at 0. For this initial study, the RMS noise was set to be equal on all segments, with a more realistic approach to segment noise applied in section 3.2, where the effects of varying RMS noise is discussed in more detail.

The results are presented numerically in Table 1, showing the average variation in search time in addition to the deviation from the known position for φ, r and z. The results clearly show that the mean deviation for all 3 parameters decrease significantly from GS 1 $\rightarrow$ GS 2 with a smaller change occurring from GS 2 $\rightarrow$ GS 3. In addition, the time taken to search a single position increases more than 10 fold from GS 1 $\rightarrow$ GS 3. The major difference between the results arises from the improved reconstruction of the φ value, with the azimuthal segments containing much of the angular information. To remove the effects of a bad measurement, each position was simulated 10 times, with the average deviation presented.

The φ improvement from GS 1 $\rightarrow$ GS 2 can be accounted for by the addition of extra azimuthal information. However, the improvement in r and z resolution arises because the weighting potential for the core segment is so large that there exists a significant probability that the core segment is also the hit segment. In this scenario, the GS 1 χ^2 is calculated using information from only 2 signals, increasing the effects of one noisy trace on the overall reconstruction. With the addition of more segments in GS 2 and GS 3, the effects of this on the χ^2 calculation are reduced.

Although the data is all analysed offline, the ultimate goal of this project would to be capable of utilising Pulse Shape Analysis (PSA) techniques in

Grid Search	Event Processing	Mean Deviation (^{o} / mm)		
	Time (s)	r	φ	z
GS 1	0.057	0.0147	1.7919	0.0225
GS 2	0.256	0.0051	1.2515	0.0060
GS 3	0.499	0.0025	1.2045	0.0026

Table 1: Variation in run time per event and position resolution for 3 different combinations of segments when running the grid search algorithm. GS 1 compared the point contact, core and hit segment signals, with GS 2 including the 8 azimuthal segments and GS 3 searching over all segments. For all runs, the normalised RMS noise was set at 0.02, equivalent to a 75 keV γ-ray

an online environment, hence the importance of the search time per event.

As seen before, there exists a strong relationship between position and drift time to the point contact. Using this, the drift time can be calculated from the test pulse, with a cut applied to the database. To calculate the drift time, the start of the pulse, t_0, must be accurately determined.

Since the point contact pulse remains in the noise for much of its drift, the t_0 algorithm developed utilises the secondary charge collecting electrode output. Due to the proximity of the γ-ray interaction to the secondary collecting electrode, the output pulse exhibits a sharp initial rise enabling the starting point of the drift to be more accurately determined. This can be seen in the first interaction in Figure 5. To further exaggerate the initial rise and also dampen the baseline noise, a cumulative pulse was taken with each bin comprising of an accumulation of all prior bins. From here, a simple threshold was set to test that the pulse was starting to rise, in addition to a check to ensure that the following samples were also rising.

Once measured, a drift time cut of $dt \pm 100$ ns can be applied to the grid search, reducing the event processing time significantly. When used in combination with the GS 3 search parameters, the event time reduced from 0.499 s $\rightarrow$ 0.054 s, with the r, φ and z resolution remaining the same. A narrower time cut would further reduce the event time, however a more accurate t_0 calculation would be necessary to ensure the drift times were calculated correctly.

In addition to the drift time cut, a cut on the electron collecting electrode can be applied to further improve the search time. As seen in Figure 8, for each segment there exists a small section of the detector wherein a γ-ray interaction would result in a termination at said electrode. This can be used to reduce the search space for the grid search algorithm. Combining this with the drift time cut described above reduces the search time per event from 0.054 s $\rightarrow$ 0.019 s whilst maintaining the position resolution values seen in the GS 3 results. For all subsequent studies, the GS 3 search parameters are used in addition to the drift time and hit segment cuts.

3.2. Effects of RMS Noise

One of the main benefits of this detector is the extremely low noise induced on the signals at the point contact. As mentioned earlier, similar point contact detectors experience peak-to-peak noise values of ~1 mV, equating to a normalised RMS noise of ~1% at 150 keV. The effects of varying the noise level from 0 $\rightarrow$ 10% at 150 keV have been studied, with the results for the average deviation presented in Table 2. In addition, a position by position scan is illustrated in Figure 9. The percentage of events reconstructed, ε_{recon}, to within 1 mm is presented for each study, with the results for 1 and

2% RMS noise showing excellent reconstruction capabilities with 100% of events reconstructed to within 1 mm of the known interaction position.

Normalised	Mean Deviation (^{o} / mm)			ε_{recon}(%)	FWHM (mm)
RMS Noise	r	φ	z	< 1 mm	
0.00	0.0000	0.000	0.0000	100.0	0.00
0.01	0.0004	0.576	0.0004	100.0	0.11
0.02	0.0025	1.205	0.0026	100	0.28
0.05	0.0696	3.535	0.0531	93.0	1.33
0.10	0.3277	7.637	0.2359	40.6	3.52

Table 2: List of mean values from RMS noise simulations, showing average deviation in r, φ, z for the detector as a whole. The percentage of events reconstructed ε_{recon}, to within 1 mm is also shown.

The effects of RMS noise are clear, with each increase in noise level resulting in a significant change in the average deviation for all three components. By examining each event individually, the 3-dimensional Cartesian position variation can also be measured, providing a value more comparable to published results for current state-of-the-art detectors (6; 7). For each event, the Cartesian 3-vector between the known position and the reconstructed position was calculated as $\sqrt{\Delta x^2 + \Delta y^2 + \Delta z^2}$, where $\Delta x, \Delta y$ and Δz represent the deviation in each of the respective dimensions. The FWHM was then calculated as

$$FWHM = 2.35\sigma = 2.35\sqrt{\frac{\sum_N \Delta^2_{x,y,z}}{N}} \tag{3}$$

where $\Delta_{x,y,z}$ is the Cartesian 3-vector. The position resolution was calculated as 0.105, 0.281, 1.332 and 3.515 mm for 1, 2, 5 and 10 % RMS noise respectively. This is substantially better than the current ∼4.5 - 5 mm attainable by AGATA at 1.3 MeV (6) and GRETINA at 2 MeV (7).

Figure 9 shows the distribution of the erroneous reconstructions follows the segmentation scheme seen in Figure 8, with the increase in RMS noise showing this effect more clearly. The addition of a segment cut results in a larger error near the centre of segments, with the errors on the boundaries significantly reduced. This plot also shows the much greater resolution in z than r, with the cut on drift time providing a clear z position for the front end of the detector. The r resolution arises in part due to the cut on segment, with the core segment showing the worst resolution in r as a consequence of its size. The resolution in φ is poorest near $r = 0$ mm, something that is likely caused by the much smaller deviation in drift time as a function of φ at small drift times, hence more similar charge pulses in these regions. It is also worth noting that larger errors in φ in these regions have less of an effect on the 3-dimensional deviation due to them being closer to the central axis. This is related to the fact that the distance, d, between two positions separated by angle, φ, at a constant radius, R, is given by $d = 2Rsin(\frac{\varphi}{2})$.

When reconstructing γ-ray tracks within a detector, the majority of interactions will be low energy Compton scatters in the 100 - 500 keV range, which when reconstructed sum to equal the initial γ-ray energy. This study shows that even at low energy, SIGMA will be capable of providing exceptional position resolution. For higher γ-ray energies, the relative contribution of the noise is reduced and hence these values will be improved upon.

One thing to consider when performing a realistic simulation is the fact that electron collecting electrodes, segments 1-19, are much larger in size than the point contact. This increased size results in a higher capacitance and hence increased series noise. To account for this, a realistic peak-to-peak noise, ranging from 5mV $\rightarrow$ 15 mV has been added to each segment according to their relative sizes. When applying this to the 1% RMS noise simulation presented in Table 2, the FWHM for the position resolution decreases from 0.11 $\rightarrow$ 0.41 mm.

3.3. Effects of Pulse Alignment

One experimental challenge to PSA lies in the ability to accurately determine the start time of the pulse, t_0. As seen earlier in Figure 7, the drift time to the point contact contains information regarding interaction position. However, due to the compact nature of the point contact weighting potential, the pulses remain near the baseline for much of that drift as shown in Figure 4. This increases the difficulty in determining t_0.

To study the effects of incorrectly identifying t_0, a random shift was assigned to each test pulse within the range -n...n, where n is the maximum number of samples to be shifted. The results for the mean response to an alignment shift of 0 $\rightarrow$ 4 samples, equating to 0 $\rightarrow$ 40 ns, is presented in Table 3, with Figure 10 showing the variation in the reconstructed position relative to the true position at $\varphi = 0^o$ for each position in the detector on a 1×1 mm grid. To isolate the effects of Δt_0, the RMS noise was set to 0 for this study.

Again, the results for $\Delta t_0 = 0$ show perfect reconstruction, with a Δt_0 of ± 10 ns having a significant effect on the reconstruction efficiency with 57.9% of the γ-ray interactions reconstructed to within 1 mm of the known

Δt_0 (ns)	Mean Deviation (^{o} / mm)			ε_{recon}(%)	FWHM (mm)
	r	φ	z	< 1 mm	
0	0.000	0.000	0.000	100.0	0.00
10	0.327	5.597	0.253	57.9	3.10
20	0.698	7.744	0.573	40.2	4.85
30	0.968	9.228	0.859	30.7	6.11
40	1.208	10.138	1.132	24.9	7.18

Table 3: List of mean deviation as a function of Δt_0, showing average deviation in r, φ and z for the detector as a whole. The percentage of events reconstructed ε_{recon}, to within 1 mm is also shown.

interaction position. The 3-dimensional FWHM is also reduced to 3.10 mm for $\Delta t_0 = 10$ ns, demonstrating the importance of correctly aligning experimental pulses with those in the database. As can be seen, a single channel misalignment in a 100 MHz digitiser output signal has the same effect as increasing the RMS noise to 10 %.

The importance of this effect is clear to see, with the variation in r, φ and z more than doubling from $\Delta t_0 = 10 \rightarrow 40$ ns. The percentage of events reconstructed to within 1 mm more than halved from $\Delta t_0 = 10 \rightarrow 40$ ns. The 3-dimensional position resolution is also significantly reduced at $\Delta t_0 = 40$ ns with FWHM = 7.18 mm.

To combat this, additional searches can be added to the grid search algorithm, whereby the pulses in the database are compared with the test pulse using multiple different alignments. Applying this methodology to the worst case studied, $\Delta t_0 = 40$ ns, with the search space expanded to cover shifts of up to ± 2 bins, the 3-dimensional position resolution improved from 7.18 $\rightarrow$

5.04 mm.

3.4. Expected Position Resolution

SIGMA will have a large variety of spectroscopic applications both as a standalone detector and as part of an array in conjunction with ancillary systems. The performance of SIGMA as a tracking and imaging system will vary in each case with the increased information available from ancillary detectors aiding in SIGMA's position reconstruction capabilities. Two scenarios are presented here; SIGMA as a standalone system and SIGMA in conjunction with an implantation detector as would be the case at the DESPEC experiment at FAIR. The advantages of using an implantation detector lie in the ability to perform temporal correlations between implantations in the ancillary and interactions in SIGMA. This should enable proper alignment of pulses to within a single digitiser sample, i.e. $<$10 ns.

For a more thorough understanding of the performance of SIGMA in real situations, the effects described in Section 3 must be collated using realistic values for each scenario. To create the realistic test pulses, a peak-to-peak noise of 1 mV was added to the point contact signal of each pulse. In addition, peak-to-peak noise ranging from 5 $\rightarrow$ 15 mV was added to segments 1-19. Simulations are presented fo initial γ-ray energies of 500 keV and 1 MeV. In addition to the series noise, a pulse alignment error was included to represent the expected errors for each of the 2 scenarios studied. For standalone SIGMA, a pulse alignment error of $\pm$30 ns was used with a value of $\pm$10 ns used for the simulations with an ancillary detector. In all studies, the pulses were processed through the GS 3 algorithm with cuts placed on both the drift time and hit segment with the search space extended to cover

$t_0 \pm 2$ s.

The results are presented in Table 4 showing the mean deviation in r, φ and z, along with the FWHM of the Cartesian 3-vector between the known and reconstructed positions. As a standalone detector, SIGMA will be capable of providing an exceptional position resolution of 4.54 mm at 500 keV. and 4.37 mm at 1 MeV. These values are significantly improved when SIGMA is paired with an ancillary detector capable of improving the t_0 determination of the pulses. As seen in Table 4, the FWHM for SIGMA with an ancillary detector is 0.65 mm at 500 keV and 0.33 mm at 1 MeV. These values would represent an improvement over current large volume germanium detectors. One note regarding these results is the fact that the simulations do not account for the finite size of the electron charge cloud and the resulting charge sharing effects that occur near segment boundaries. These effects will be studied in more detail during the experimental phase of this project.

	E_γ(keV)	Mean Deviation			FWHM
		r (mm)	φ (^{o})	z (mm)	(mm)
Standalone	500	0.570	7.612	0.451	4.54
	1000	0.535	7.124	0.424	4.37
w Ancillary	500	0.049	1.347	0.036	0.64
	1000	0.006	0.533	0.006	0.33

Table 4: List of mean deviation for two configurations of SIGMA at initial γ-ray energies of 500 keV and 1 MeV showing the average deviation in r, φ and z for the detector as a whole. Also presented is the FWHM for the Cartesian 3-vector between the known position and the reconstructed position.

4. Conclusion

The SIGMA detector should be capable of providing unrivalled position and energy resolution, with its unique design enabling major advancements over current state-of-the art large volume HPGe detectors used in the tracking arrays AGATA and GRETA. A limiting theoretical estimate suggests a 3-dimensional position resolution ranging from 0.41 mm at 150 keV to 0.33 mm at 1 MeV. Performance such as this will aid in drastically improving the tracking and imaging capabilities of large volume HPGe detectors. With a more accurate and consistent determination of t_0, tighter cuts on the drift time can be applied, decreasing the time taken to scan a single event in addition to providing much tighter constraints on the interaction position.

5. Acknowledgements

This research was supported by the United Kingdom Science and Technology Facilities Council (STFC UK) grant ST/M003582/1 and the U.S Department of Energy, Office of Science, Office of Nuclear Physics, under contract number DE-AC05-00OR22725. The authors would also like to acknowledge the contributions of Karin Lagergren, Ren Cooper and Heather Crawford.

[1] R. Cooper et al., A novel HPGe detector for gamma-ray tracking and imaging, Nuc. Instr. Meth. A 665 (2011) 25–32.

[2] M. Salathe et al., Energy reconstruction of an n-type segmented inverted coaxial point-contact HPGe detector, Nucl. Instr. Meth. A 868 (2017) 19–26.

[3] B. Rubio, Decay Spectroscopy (DeSpec) at the New FAIR-NuSTAR Facility, Int. Jour. Mod. Phys. E 15 (2006) 1979–1988.

[4] L. Harkness-Brennan et al., An Experimental Characterisation of a Broad Energy Germanium Detector, Nucl. Instr. Meth. A 760 (2014) 28–39.

[5] K. Vetter et al., Three-dimensional Position Sensitivity in Two-dimensionally Segmented HPGe Detectors, Nucl. Instr. Meth. A 452 (2000) 223–238.

[6] F. Recchia et al., Position resolution of the prototype AGATA triple-cluster detector from an in-beam experiment, Nucl. Instr. Meth. A 604 (2009) 555–562.

[7] M. Descovich et al., In-beam measurement of the position resolution of a highly segmented coaxial germanium detector, Nucl. Instr. Meth. A 553 (2005) 535–542.

[8] D. Radford, et al., FieldGen/SigGen software, available by svn at `http://radware.phy.ornl.gov/MJ/ic_siggen/`.

[9] W. Shockley, Currents to Conductors Induced by a Moving Point Charge, J. Appl. Phys 9 (1938) 635.

[10] S. Ramo, Currents Induced by Electron Motion, Proceedings of the I.R.E September (1939) 584.

[11] Z. He., Review of the Shockley-Ramo theorem and its application in

semiconductor gamma-ray detectors, Nucl. Instr. Meth. A 463 (2000) 250–267.

[12] L. Mihailescu et al., The influence of anisotropic electron drift velocity on the signal shapes of closed-end HPGe detectors, Nucl. Instr. Meth. A 447 (2000) 350–360.

[13] S. Akkoyun, et al., Nucl. Instr. Meth. A 668 (2012) 26.

[14] G. Schmid et al., A γ-ray tracking algorithm for the GRETA spectrometer, Nucl. Instr. Meth. A 430 (1999) 69–83.

[15] W. Jung, Op Amp Applications Handbook, Newnes, 2002.

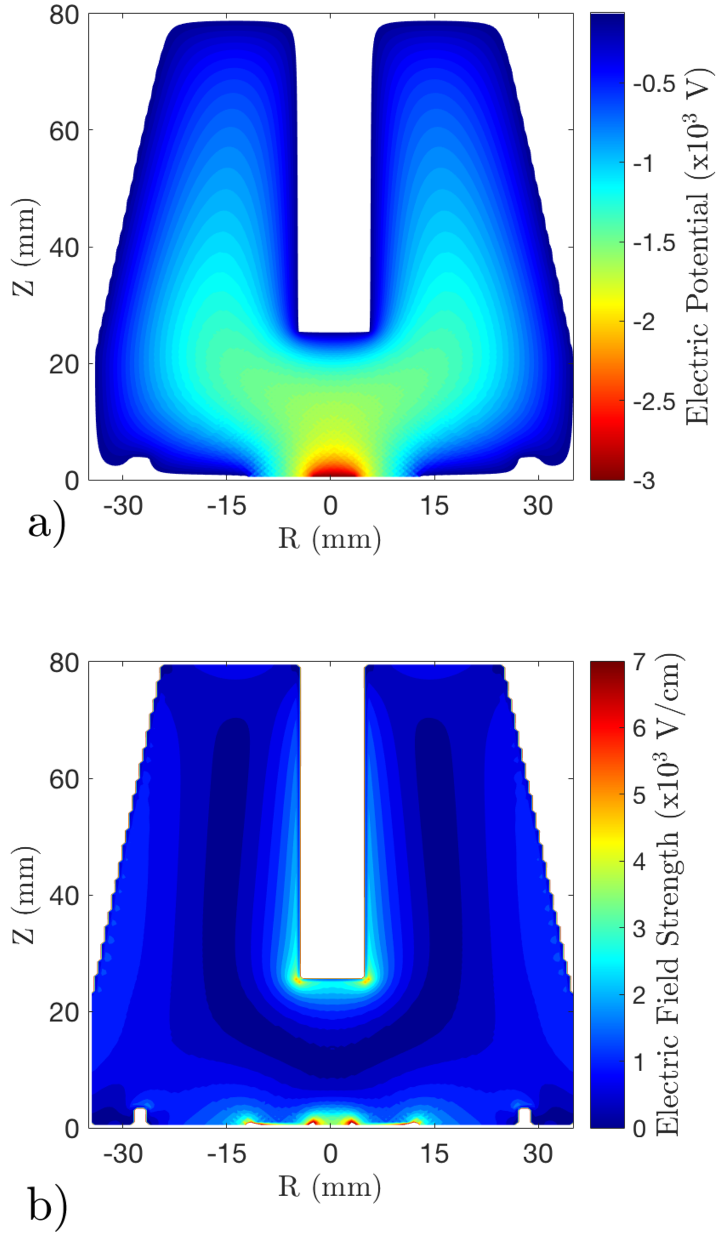

Figure 3: (a) The simulated electric potential and (b) the simulated electric field strength of the SIGMA detector showing the short range of the electric potential and also the very weak fields present in the bulk of the crystal (colour online).

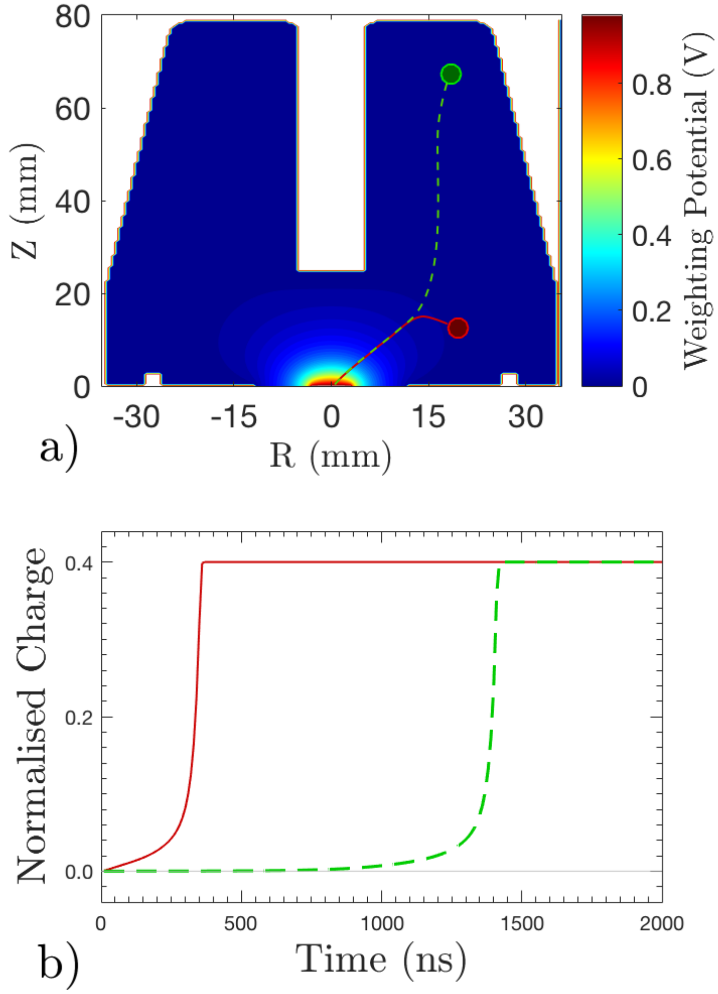

Figure 4: (a) The weighting potential for the point contact and (b) two example point contact charge pulses resulting from γ-ray interaction occurring in different locations within the detector. The red (solid) and green (dashed) circles in (a) represent the positions of the two γ-ray interactions that produce the signals shown in (b) with the charge drift paths overlaid. There exists a clear temporal variation in the signals; a feature that enables multiple interactions to be more easily identified (colour online).

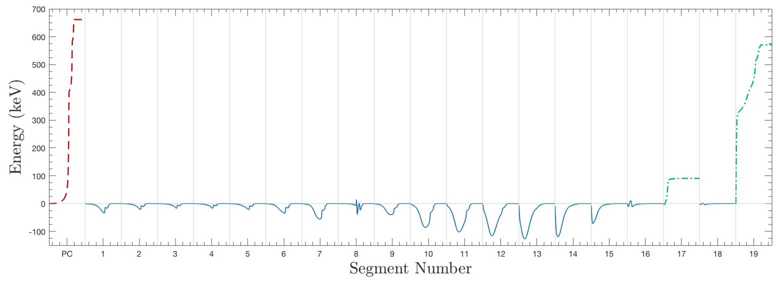

Figure 5: Example pulses from a multi site event interacting in the SIGMA detector. The terminating electrode of the holes and electrons are highlighted in red (dashed) and green (dot-dashed) respectively, with all image charges shown in blue (solid) (colour online).

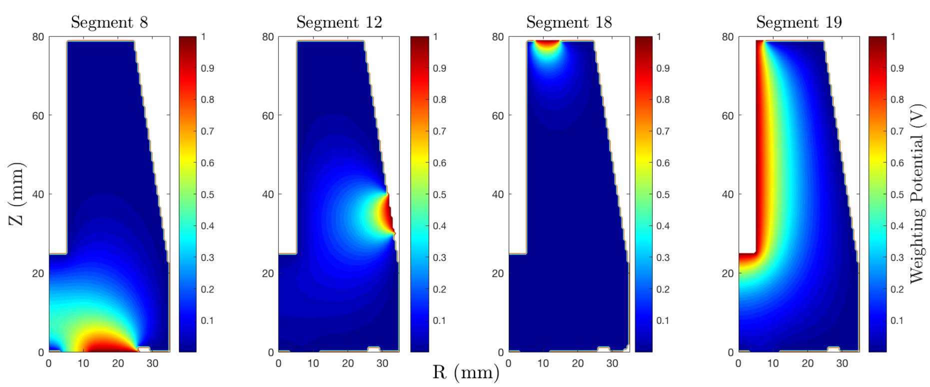

Figure 6: Simulated weighting potentials through the central axis for four segments in the SIGMA detector. Only 1 potential is calculated for the azimuthal segments with the same potential used for each (colour online).

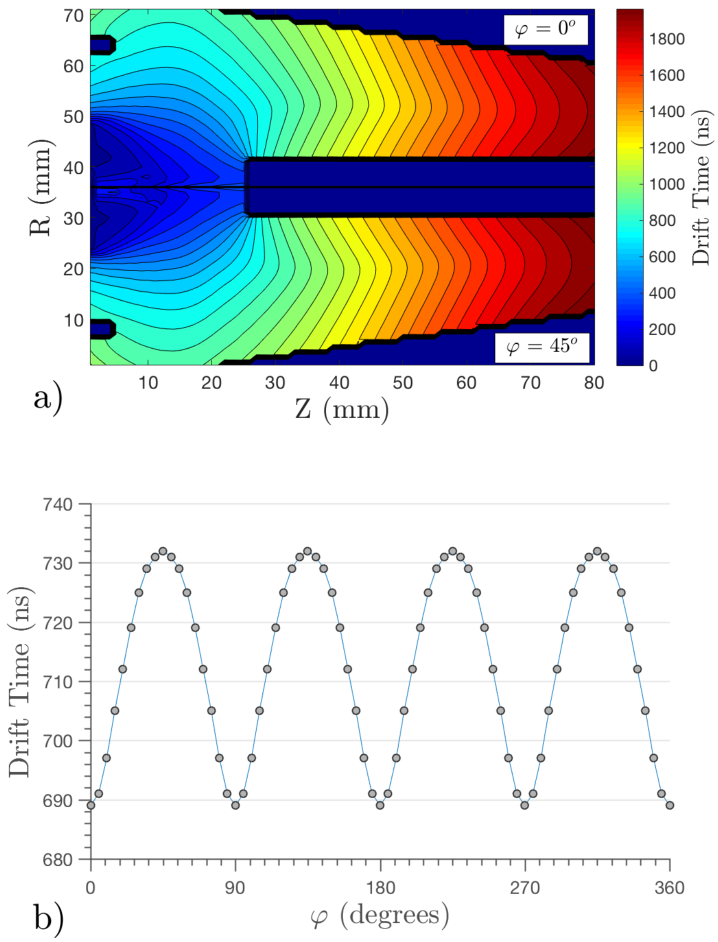

Figure 7: (a) Drift time distribution as a function of γ-ray interaction position within the detector. Overlayed are 50 ns isochrones. The top half of the figure shows results for $\varphi = 0^o$, with the lower half showing $\varphi = 45^0$, with a slight variation seen in the drift patterns between the two as a result of the change in crystallographic axis with varying φ. (b) Variation in drift time as a function of φ for a γ-ray interaction at $(r, z) = (20, 20)$ mm, showing the ∼6 % peak-to-peak change from $0^o \rightarrow 45^o$ (colour online).

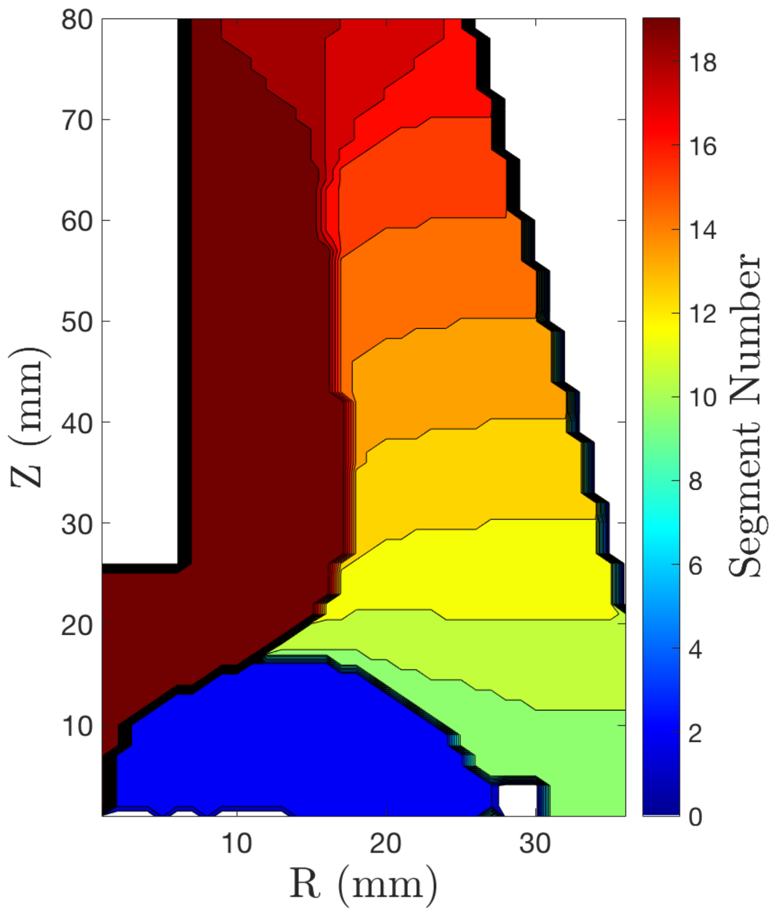

Figure 8: Illustration of the secondary collecting electrode as a function of γ-ray interaction position within the detector (colour online).

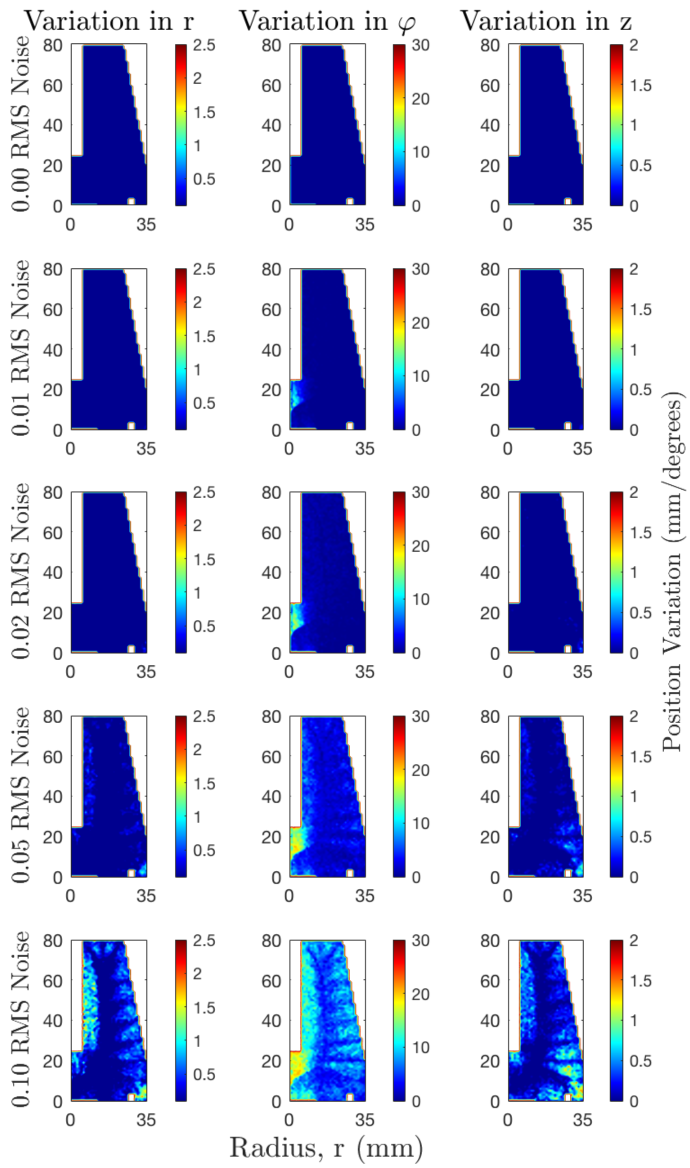

Figure 9: Deviation of reconstructed position from true position as a function of RMS noise, using the GS 3 algorithm in addition to cuts placed on the drift time (± 100 ns) and hit segment. Deviations for r, φ and z are shown in the left, middle and right panels respectively in units of mm and ^{o} (colour online).

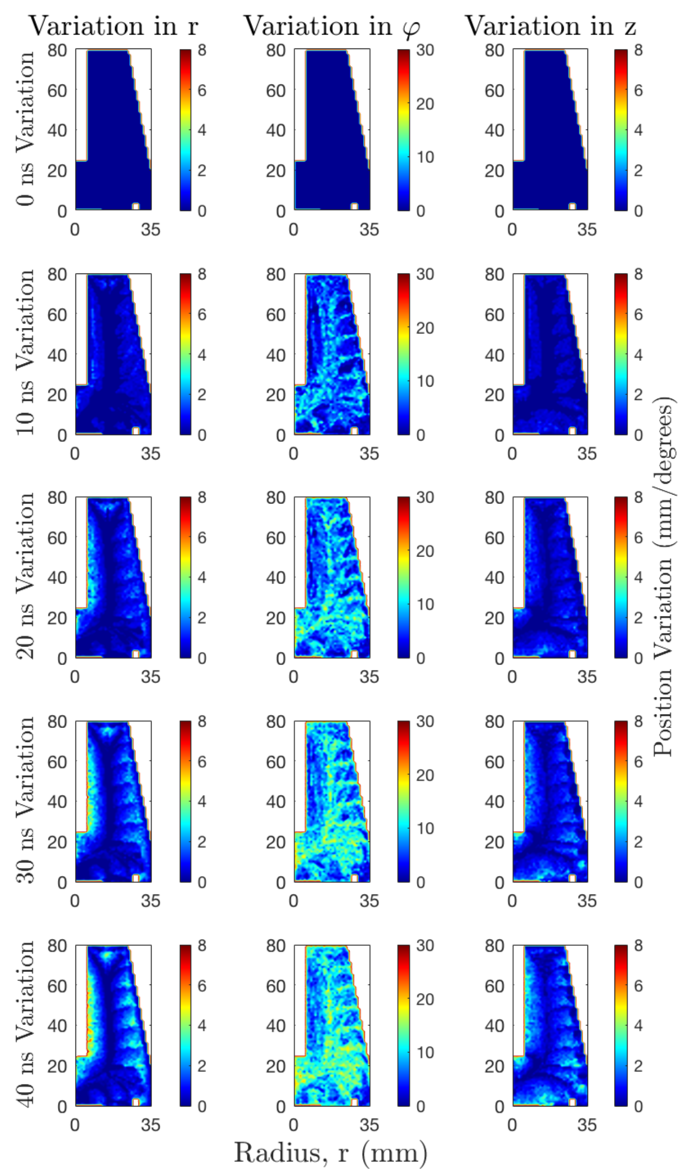

Figure 10: Deviation of reconstructed position from true position as a function of pulse alignment error, using the GS 3 algorithm in addition to cuts placed on the drift time ($\pm$ 100 ns) and hit segment. Deviations for r, φ and z are shown in the left, middle and right panels respectively in units of mm and ^{o} (colour online).

Figure1

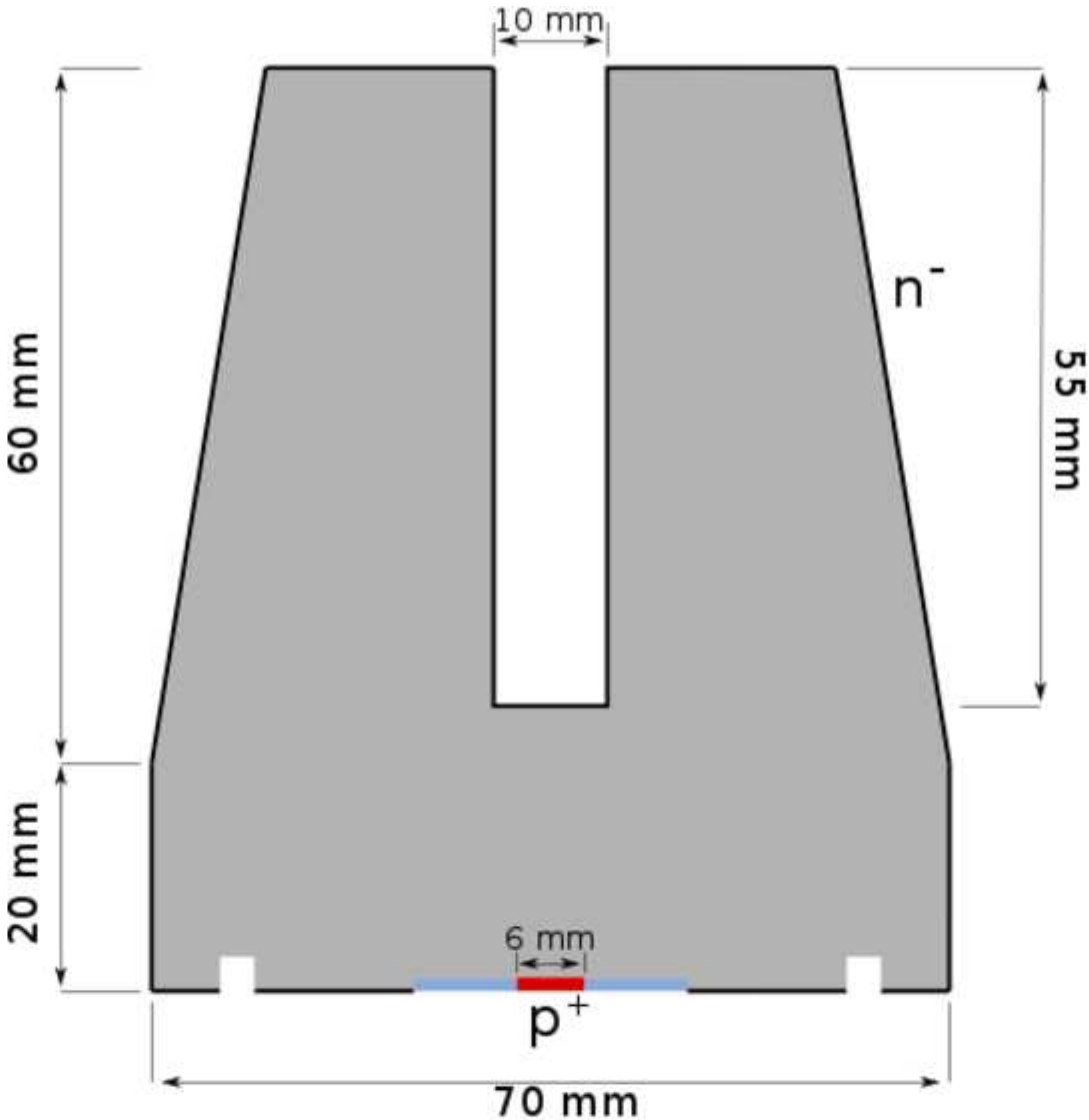

Figure2

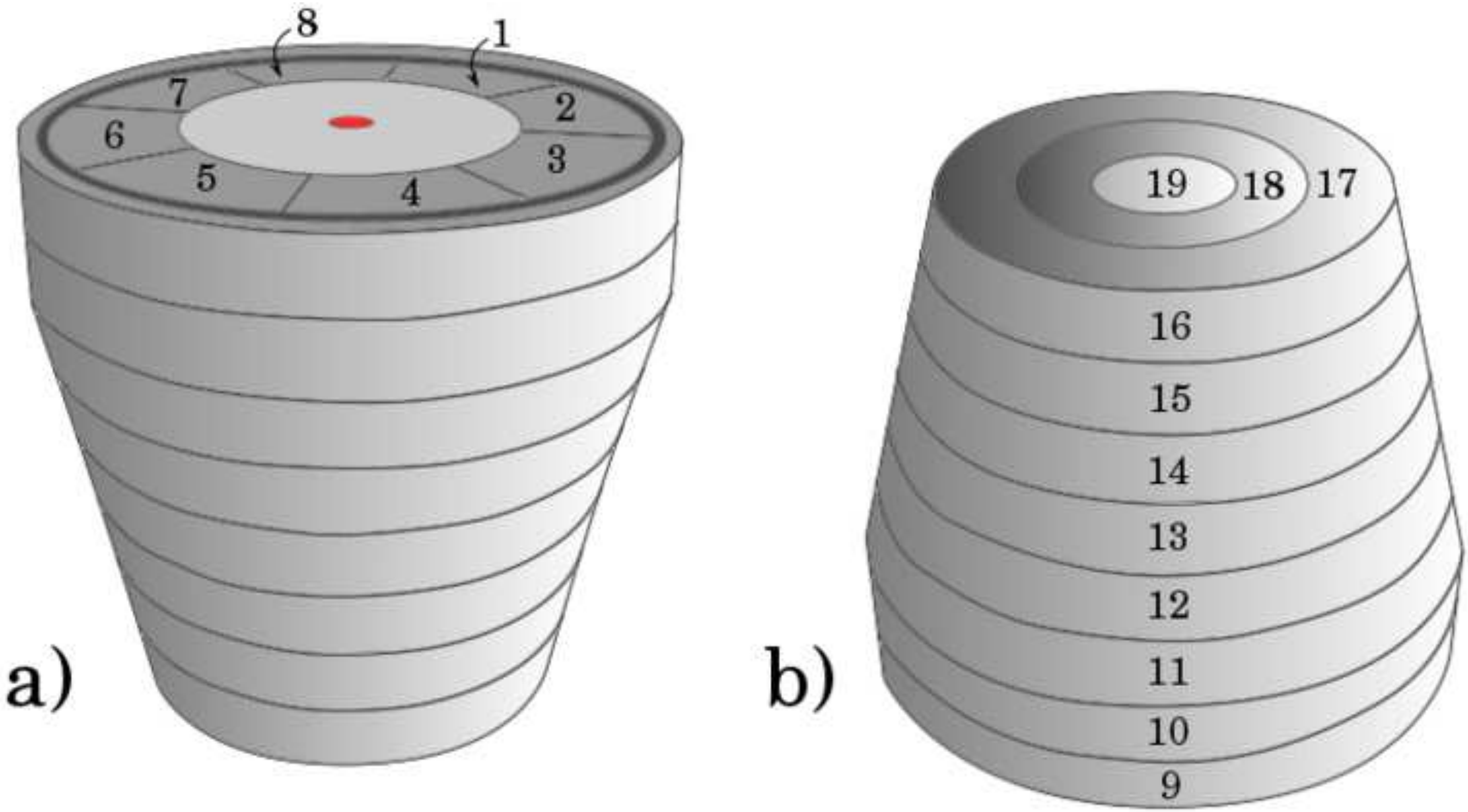

Figure3

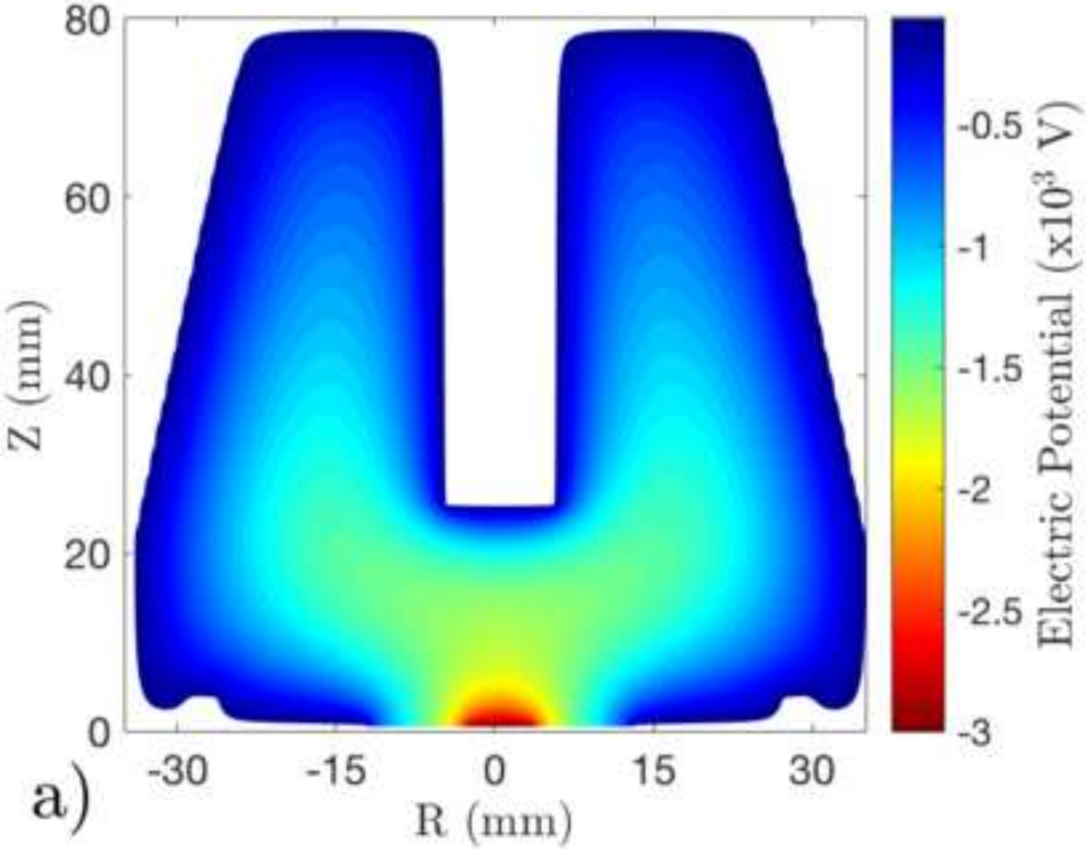

80
60
40
20
0
Z (mm)
-30
-15
0
15
30
R (mm)
a)
-0.5
-1
-1.5
-2
-2.5
-3
Electric Potential (x10^3 V)

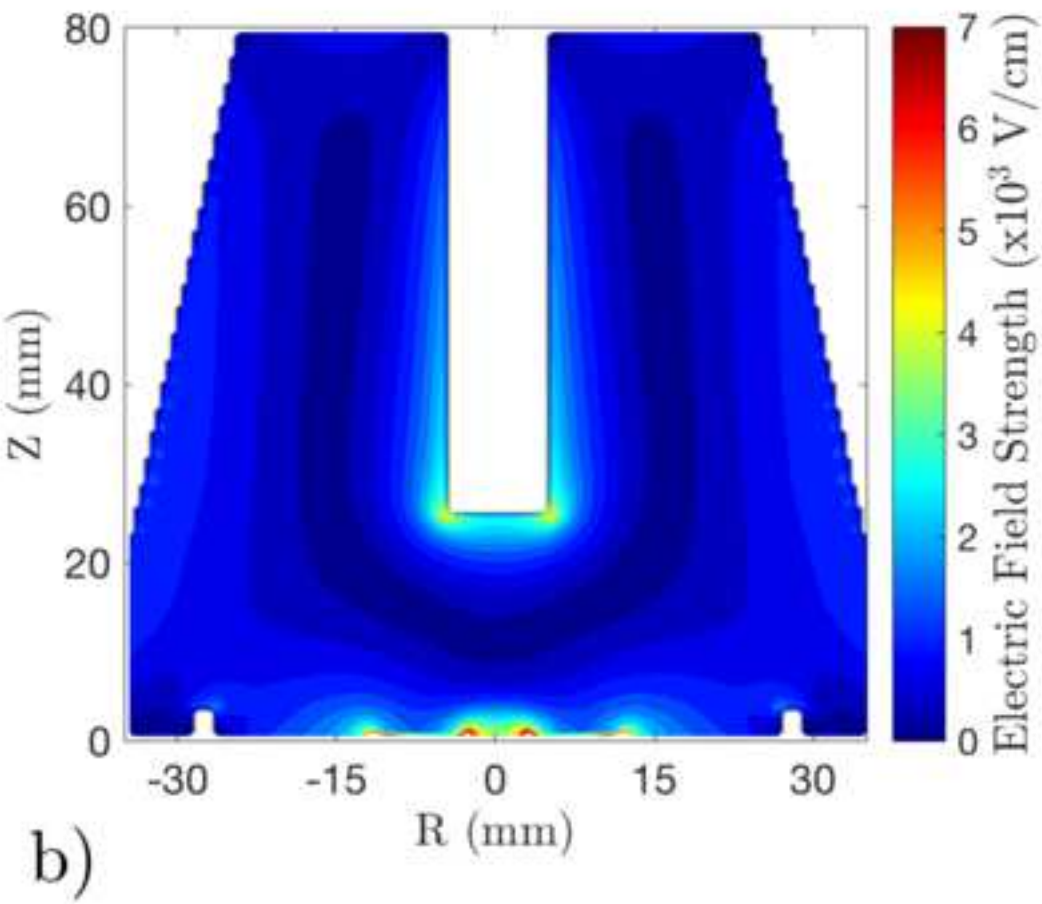

80
60
40
20
0
Z (mm)
-30
-15
0
15
30
R (mm)
b)
7
6
5
4
3
2
1
0
Electric Field Strength (x10^3 V/cm)

Figure4

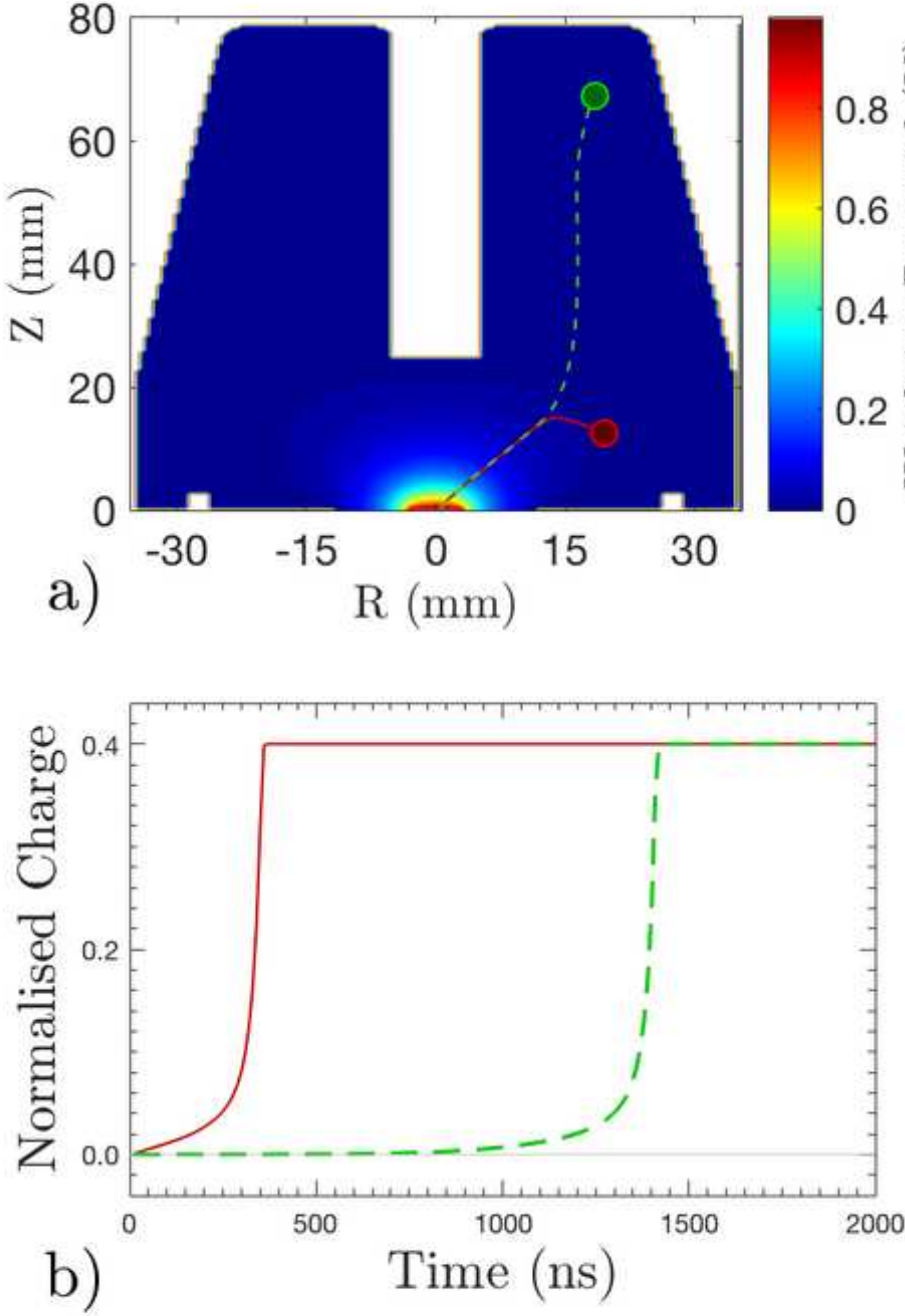
80
60
40
20
0
Z (mm)
-30
-15
0
15
30
R (mm)
0.8
0.6
0.4
0.2
0
Weighting Potential (V)
a)
0.4
0.2
0.0
Normalised Charge
0
500
1000
1500
2000
Time (ns)
b)

Figure 5

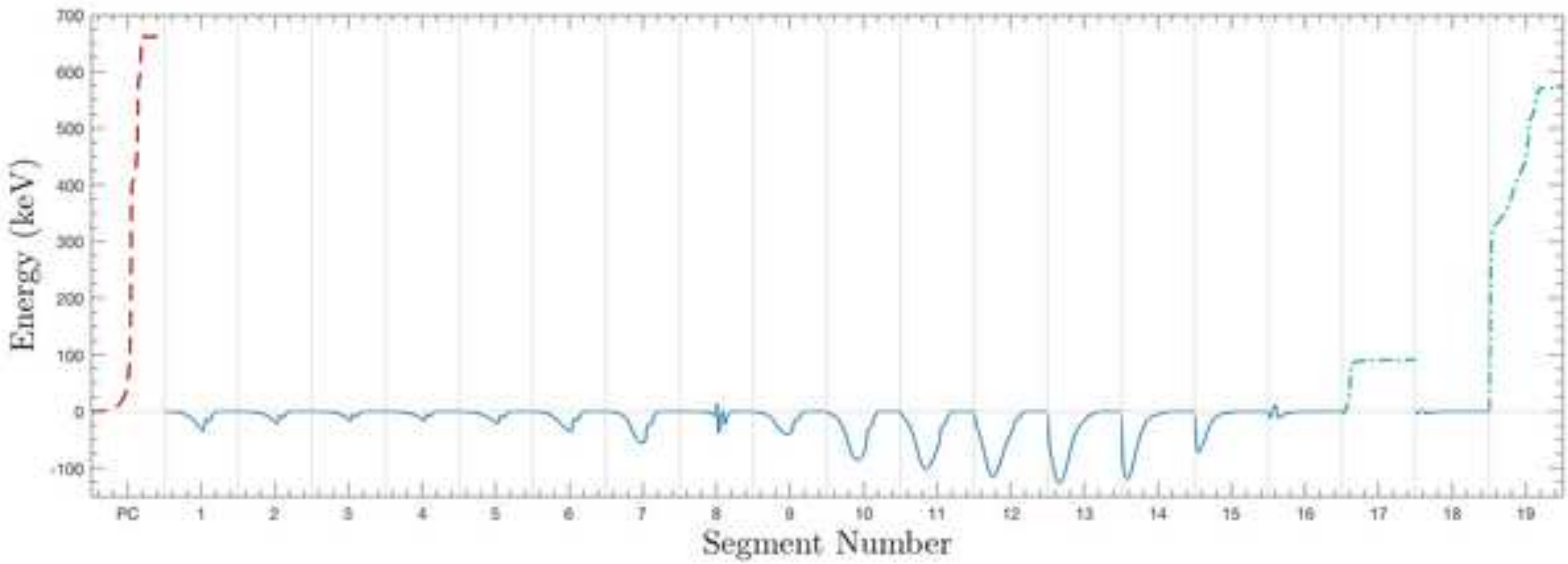

Energy (keV)
700
600
500
400
300
200
100
0
-100
PC
1
2
3
4
5
6
7
8
9
10
11
12
13
14
15
16
17
18
19
Segment Number

Figure6

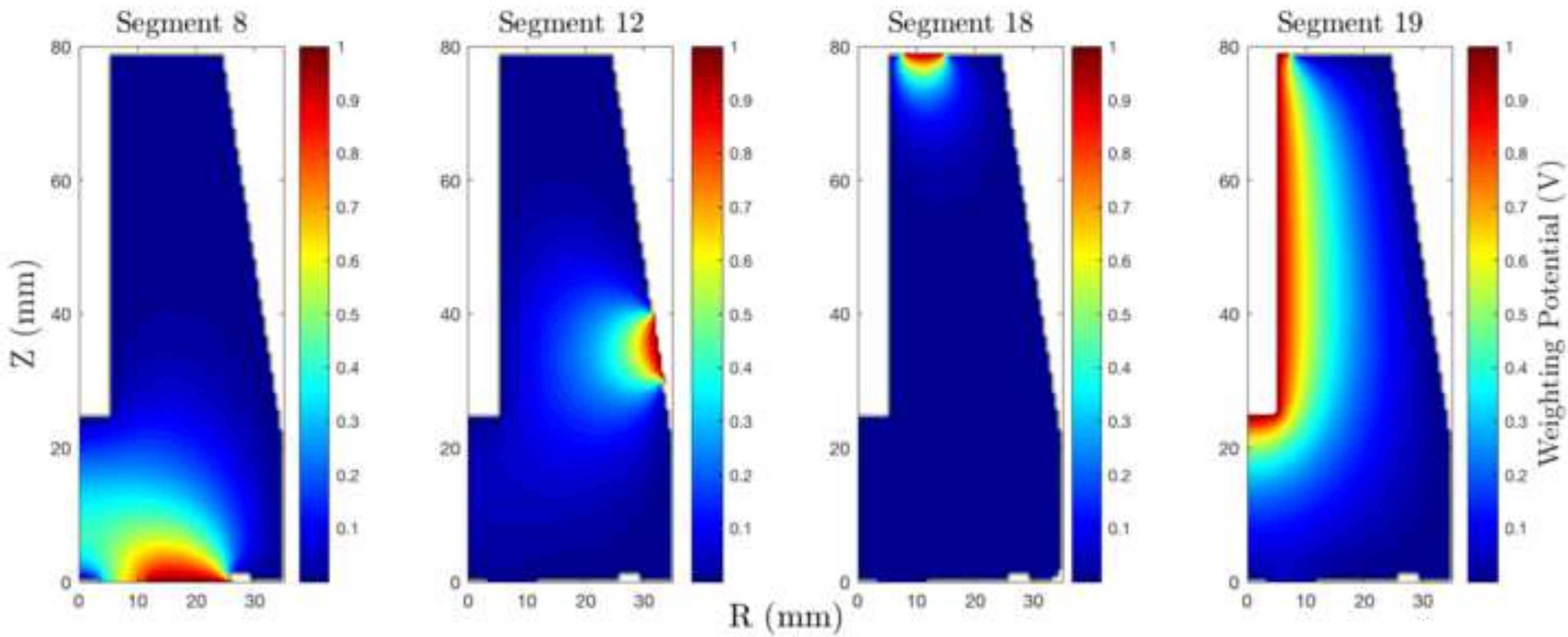
Segment 8
Segment 12
Segment 18
Segment 19
Z (mm)
R (mm)
Weighting Potential (V)
0
10
20
30
40
60
80
0.1
0.2
0.3
0.4
0.5
0.6
0.7
0.8
0.9
1

Figure7

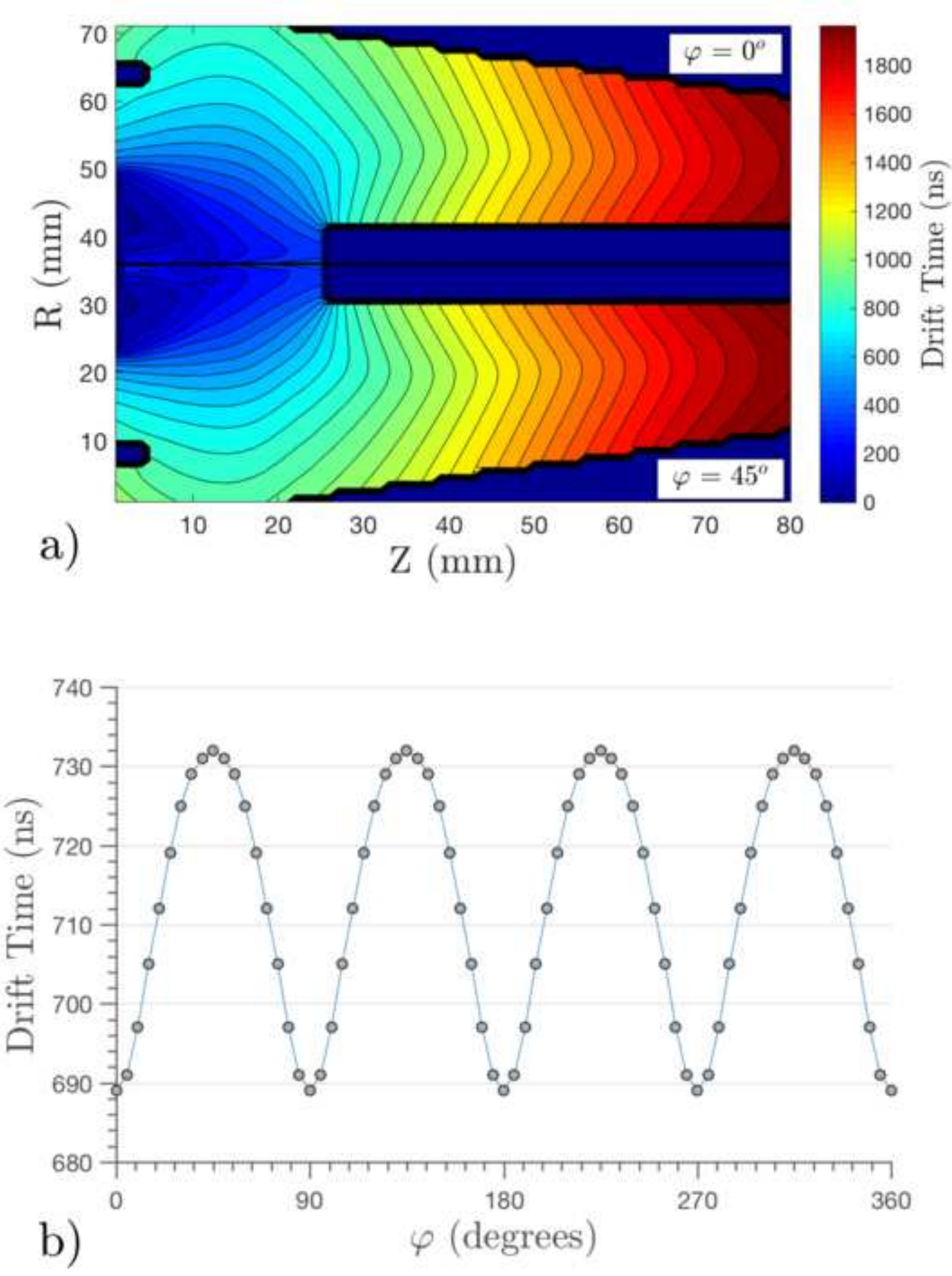

φ = 0°
φ = 45°
R (mm)
Z (mm)
Drift Time (ns)
70
60
50
40
30
20
10
10
20
30
40
50
60
70
80
1800
1600
1400
1200
1000
800
600
400
200
0
a)
740
730
720
710
700
690
680
0
90
180
270
360
φ (degrees)
Drift Time (ns)
b)

Figure8

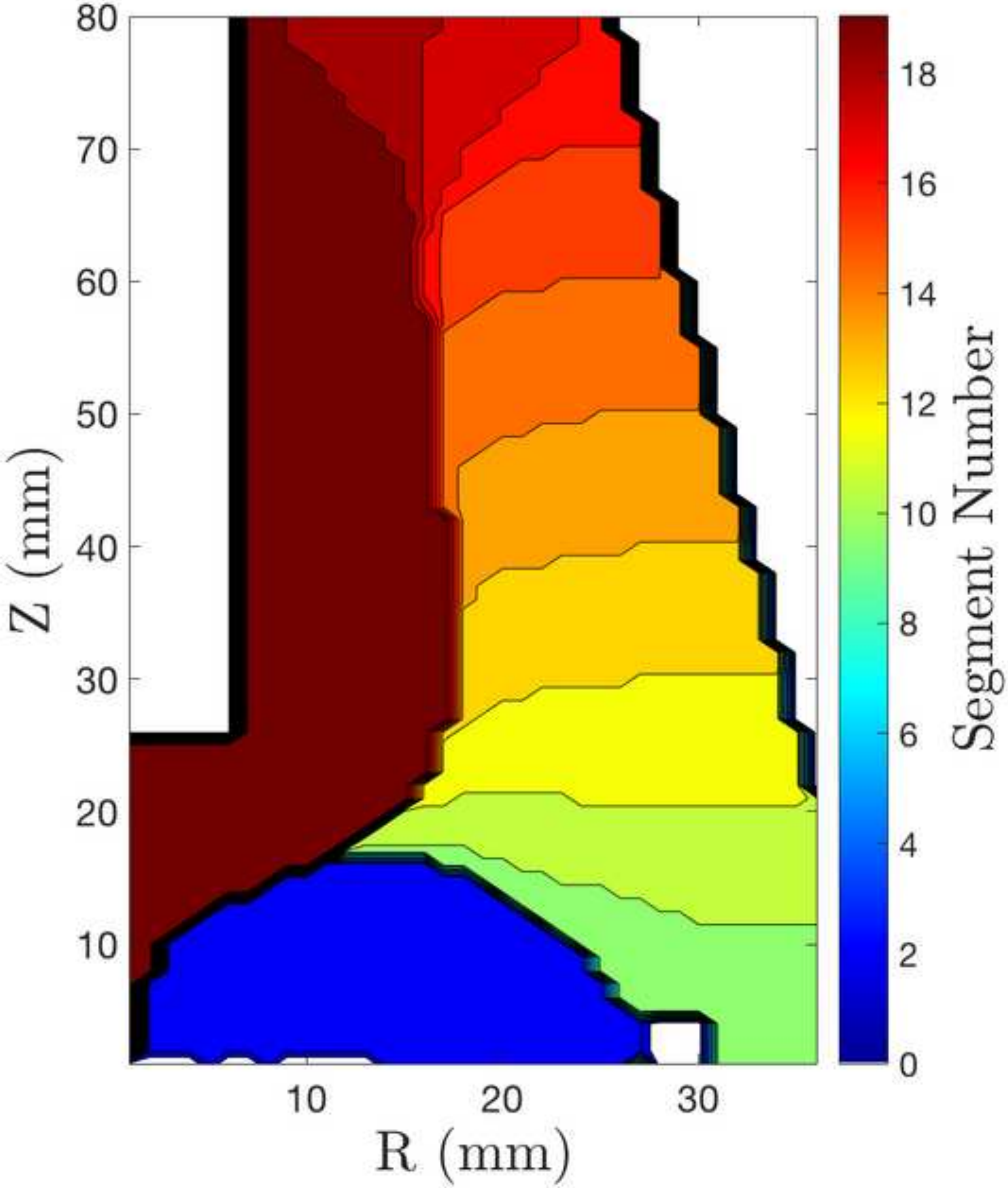
80
70
60
50
40
30
20
10
Z (mm)
10
20
30
R (mm)
18
16
14
12
10
8
6
4
2
0
Segment Number

Figure9

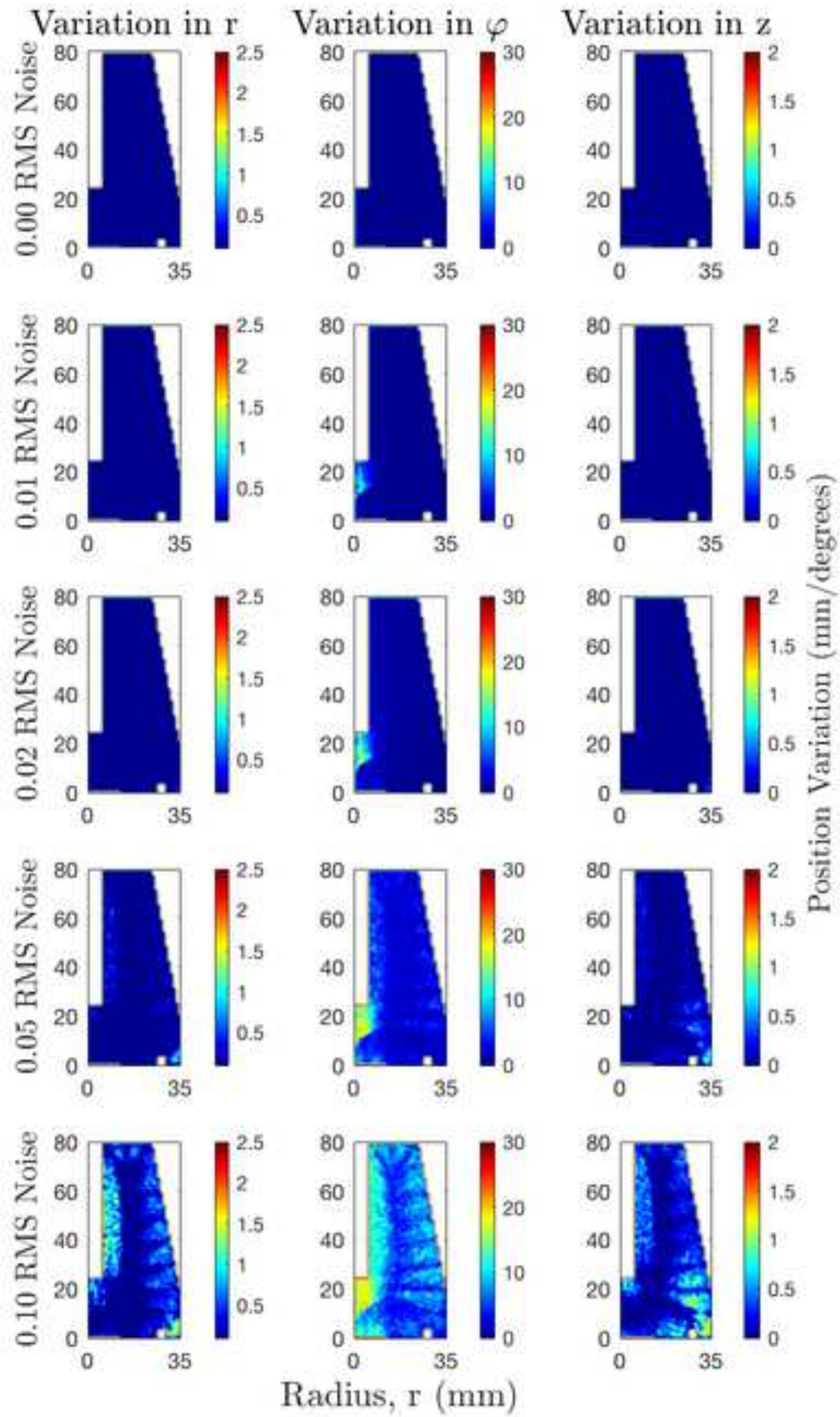
Variation in r
Variation in φ
Variation in z
0.00 RMS Noise
0.01 RMS Noise
0.02 RMS Noise
0.05 RMS Noise
0.10 RMS Noise
80
60
40
20
0
0
35
2.5
2
1.5
1
0.5
30
20
10
0
2
1.5
1
0.5
0
Position Variation (mm/degrees)
Radius, r (mm)

Figure10

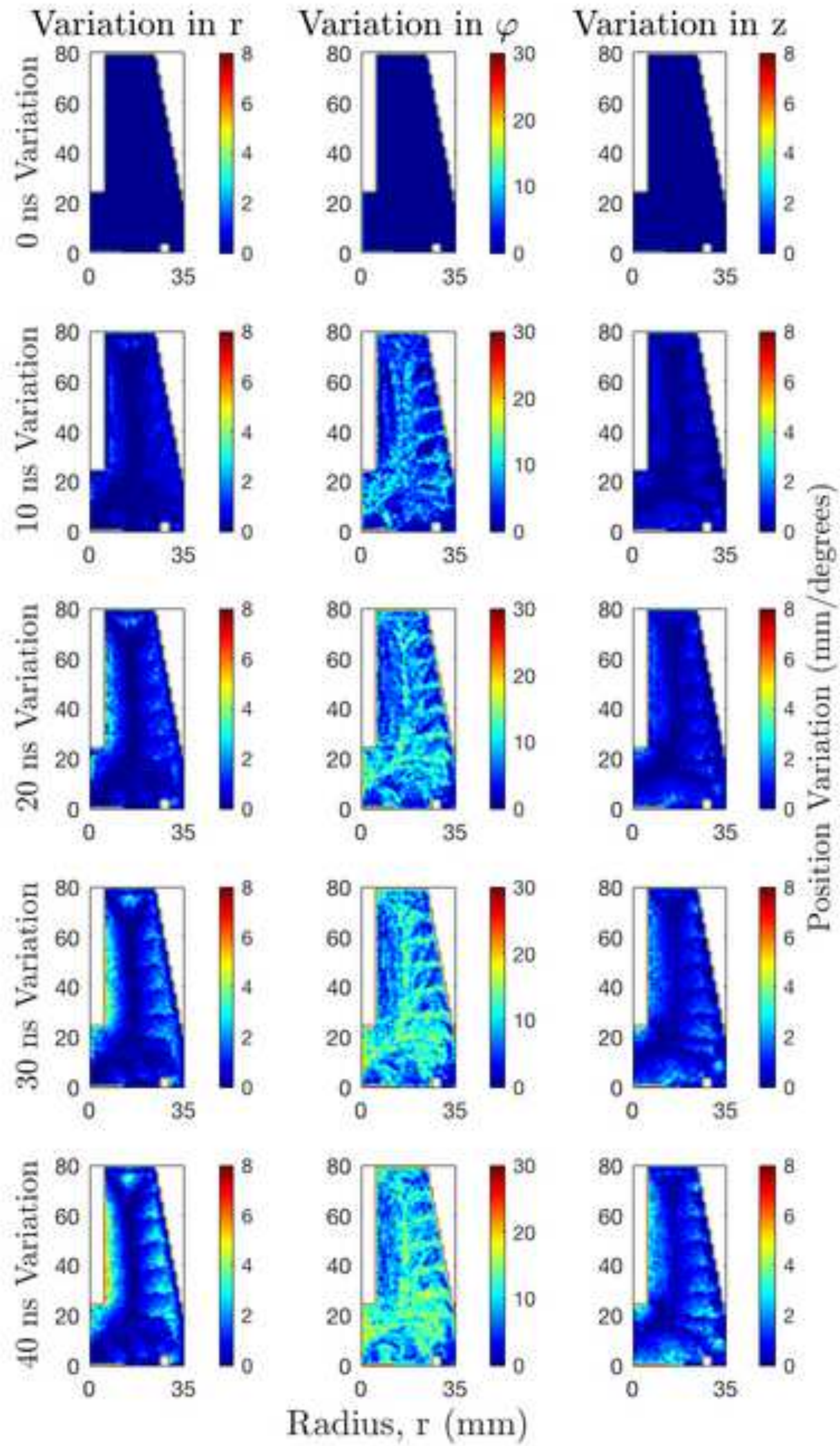

Variation in r
Variation in φ
Variation in z
0 ns Variation
10 ns Variation
20 ns Variation
30 ns Variation
40 ns Variation
Position Variation (mm/degrees)
Radius, r (mm)

Response to reviewers **Reference: NIMA-D-17-01100**

Submitted: "Position Resolution Simulations for the Inverted-coaxial Germanium Detector, SIGMA"

Corresponding author: Dr Jonathan Wright

The authors would like to thank the reviewers for providing constructive feedback on the submitted article. We are pleased that reviewer 1 has recommended the work for publication, following a few small modifications. We would like to respond to each of the comments and identify the actions taken to improve the article.

Reviewer 1:

The first reviewer has provided detailed comments, which have been addressed by the authors:

1 – Page 2 line 27 :

> *"One of the benefits of point-contact detector is the reduced capacitance (1 pF) of the electrode when compared to that of standard coaxial detector. It would be more informative to mention the corresponding capacitance value for standard detectors in the manuscript."*
> The only information we have on coaxial detector capacitance has been given in confidence therefore exact values cannot be relayed. To provide scale "(~10's of pF)" has been added to the text.

2 – Page 2 line 34 :

> *"BeGE is not defined while it is done later on, at line 235. Should be corrected."*
> Definition has been removed from line 235 and added to line 34.

3 – Page 3 line 42 :

> *"the authors should elaborate more about the location of the position interaction within less than a 1 mm. Is this performance expected with any pulse shape analysis algorithm or with a specific one? If so this should be emphasized."*
> The performance of PSA algorithms will depend upon the variation in signal shapes. The algorithm used for this work was a FoM minimisation technique but the signal variation in SIGMA is what provides the improvement over other HPGe detectors. More advanced algorithms should provide at least the same levels of performance.

4 – Page 3 line 44 :

> *"Ref.5 corresponds to in-beam position resolution of AGATA whereas ref.6 is not. I would suggest M. Descovich et al, NIM 533 (2005)535 as the proper reference 6."*
> Reference 6 has been replaced throughout the document.

5 – Page 3 line 58 :

"the passivation region as mentioned in the text, is not clearly seen in Figure 1. The authors can easily modify the figure to make it clear for the reader."

Figure 1 has been altered so that the passivation region is highlighted in blue. Text altered correspondingly to alert the reader to this.

6 – Page 5 line 75 :

" "segments 17&18 " should correctly written as "segments 17 and 16" "

Corrected.

7 – Page 5 :

"Ref 7 and 8 correspond to the same web page link and hence should be merged into a single reference."

Corrected.

8 – Page 6 line 93-94 :

"The operational voltage as measured by the manufacturer is NOT slightly higher compared to simulated full depletion. The authors should rephrase this sentence and elaborate more regarding about the difference of 1000 Volts."

We agree that this sentence was phrased in a confusing manner and have therefore reworded it.

9 – Page 7 line 105 :

"miss-spelling of upto -> up to"

Corrected.

10 – Page 8 :

a) *"Fig4 shows two examples of point contact pulses for the chosen interaction points. To be consistent with Reference 1, the authors should/could also display the outer segment and core contact pulses. In addition, it is stated that due to the sharp rising edge, it is much easier to differentiate multiple interactions than in a comparable coaxial detector. Is this statement valid for any position of the interactions? If one chooses a very close interactions points near the green or the red circles, how does the super pulse change?*

b) *Figure5 shows an example of full trace and it is not clear whether it corresponds to the interactions that are displayed in Fig4. In addition, Fig5 displays a signal distortion around segment 8 that I don't understand. Could the authors elaborate on that?"*

c) *At line 144, the difference in pulse quality is pointed out but I don't see any comparison with another super pulse (for example when using an AGATA crystal) that illustrates this quality."*

a) The purpose of Figure 4 is to illustrate the temporal variation in the point contact pulse as a function of position which does not require the core and outer segment pulses. Examples of pulses from all segments are shown in Fig 5.
   For nearby interactions, a superposition will occur in the point contact trace however the drift time varies significantly over short distances; thus enabling the two pulses to be identifiable. The two pulses in Figure 4 where chosen so this effect was clearly visible to the naked eye and not just identifiable through computer based analysis.
b) The full trace shown in Figure 5 is for a multi site event, i.e. a single photon that has scatter multiple times within the crystal, whereas the interactions in Figure 4 are singles used to illustrate the temporal variation in the point contact trace as a function of position. They do not correspond to the interaction positions shown in red and green. The signal distortion in segment 8 is likely a result of multiple charge carriers from the multiple interactions (2 x scatter + PE absorption) drifting in opposite directions through the weighting potential of segment 8. The same effect is seen in all segments to varying degrees, however the larger induced charges dilute the visibility of this to the naked eye.
c) Added a reference to *S.Akkoyun et al., NIM A668(2012)26* where example pulses are presented.

11 – Page 10 :

"Figure 8 as an extension of the results of Fig.6 is not clear and the final collecting electrode versus the position of the interaction is not obvious for a general reader. I would suggest and improvement of this section together with a correction of typos than one sees on the labels of Fig.8."

The section has been reworded to make it more accessible to a general audience as described below. The label on Fig.8 has been corrected.

Original:

To understand the drift paths of the electrons in this detector, the final collecting electrode of the electron is plotted as a function of γ-ray interaction position in Figure 8. This plot is an extension of the results in Figure 6 providing a clearer image of the relative influence of each electrode on charge collection path. The scale of the core contact is clear to see, with most interactions occurring near the central axis of the crystal terminating the core. However for interactions occurring far from the central axis of the detector, there are clearly defined bands representing each of the outer contacts.

New:

To understand the drift paths of the electrons in this detector, the electron collecting electrode, outer hit segment, is plotted as a function of γ-ray interaction position in Figure 8. The relative sizes of each of the segments in Figure 8 are a direct result of the relative strengths of the weighting potentials shown in Figure 6 and provide a clearer image of the relative influence each electrode has on the charge collection path. The scale of the core contact is clear to see, with most interactions occurring near the central axis of the crystal terminating the core. However for interactions occurring far from the central axis of the detector, there are clearly defined bands representing each of the outer contacts.

12 – Page 10 line 186 :

"references should be added for the performance of gamma-ray tracking versus the accurate measurements of the interaction point positions and energies."

Added reference to *G.J. Schmid, et al.,NIM A430(1999)69-83* which explains the effects of both energy and positions resolution on the performance of a tracking algorithm used for GRETA. More specifically, this paper explains how the errors in the position and energy of the gamma-ray corresponds to the errors in the individual parameters used in the tracking algorithm.

13 – Page 10 line 191 :

"a reference for the grid search algorithm is suitable"

The grid search algorithm used is a simple exhaustive grid search with all modifications outlined in the text. The FoM minimisation is a standard mathematical procedure.

14 – Page 10 Line 199 :

"outputted is probably an incorrect word and should be corrected."

Changed from "pulses directly outputted by SigGen" to "pulses directly generated from SigGen"

15 – Page 11 line 205 :

" "A grid search algorithm" to be replaced by " A grid search (GS) algorithm " in order to make the reader understanding what is referred to as GS1, GS2 and GS3."

Altered.

16 – Page 11 line 209 :

"S^m_ij being the measured pulses over the number of segments is confusing since all the work presented in this paper is based on simulated data. The authors should correct this."

Changed S^m to refer to modified pulses instead of measured.

17 – Page 12 line 228 :

"1 mm x 1 mm x 3^o grid. I Guess this a 1 mm x 3^o x 1 mm grid that corresponds to (r,phi,z). Is a 3 degrees small enough? What one would expect when using 1mm x 1 deg X 1 mm grid basis?"

That is correct. The effects of using a 1^o grid has been investigated and the results showed no statistically significant variation from those presented. This results from the variation in drift time over 3^o being less than the drift time variation over 1 mm in R and Z, therefore the gains from a finer phi grid are lost in the errors from the R,Z grid. Given the difference in computation power required for the smaller grids, it was decided to use the larger grid for the study presented.

18 – Page 12 line 236 and 238 :

"the authors should choose between a single notation for consistency : either peak-to-peak or Peak-to-Peak in the entire text."
Corrected.

19 – Page 13 line 267 :

"a reference for the PSA should be added unless the authors refer to the GS algorithm."
I have added the reference *K.Vetter, et al.,NIM A452(2000)223-238* for the use of PSA as a means of improving position resolution through the use of charge pulses.

20 – Page 14 line 272 :

"a simple and a more complex t_0 algorithm is not clear and should be explained in more details. Did the authors investigate the effect of applying the Kolmogorov-Smirnov method (EPJA 40(2009)249?"
The sentence was ambiguous and has been removed. The method used, as described in the text, worked sufficiently well for this study and provides us with a reference for future work. The method in question was not investigated, however such methods may be looked at when we begin optimising the PSA process and start to analyse experimental data.

21 – Page 16 line 316 :

"the reference to the mentioned published results is missing."
Reference is to AGATA/GRETINA papers discussed earlier. They have been added.

22 – Page 17 line 323 :

"The comparison of the position resolution as obtained in this work and those obtained with AGATA and GRETINA is not consistent. F. Recchia paper refers to an energy of 1.3 MeV whereas for GRETINA one refers to a 2 MeV line."
Added the energies of each study to provide clarity to the reader. It is expected that higher energy signals will produce better performance due to the increased signal-to-noise ratio on the pulses and therefore SIGMA will give at least the quoted values or better if a higher energy study were to take place.

23 – Page 21 line 412 :

"unit for t0 is missing"

line 417 :

"full stop is missing between "1 MeV" and "These values" "
Corrected.

24 – Page 21 Table 4 :

“when using SIGMA in a standalone mode, a tiny difference is seen in the achieved FWHM at 0.5 and 1 MeV (4.54 versus 4.37 mm). However, when SIGMA is used with an ancillary detector indeed one notices the improvement; but one also gets about 50% difference (0.64 versus 0.33 mm): Is there an explanation for this?”

The effects of the time alignment are much more significant than the effects of the factor 2 change in RMS noise from 1 MeV -> 500 keV. Refer to the results from the RMS and Pulse Alignment studies for confirmation of this.

25 – Conclusion :

“The conclusion emphasizes the unprecedented position resolution obtained with sigma and such this would help AGATA and GRETA tracking rays improve their performance. If so, what is the current limitation of point contact detector that makes it not usable for AGATA and GRETA yet?”

As with the AGATA and GRETINA arrays, technical evolution in the manufacturing of novel detectors is required. A prototype n-type detector is currently under investigation, *M.Salathe et. al, NIM A868(2017)19-26,* and the p-type discussed here is currently being manufactured. Once the performance of both detectors are experimentally validated, it is expected they will offer a step change in array performance as predicted by the work in *R.Cooper et. al, NIM A665(2011)25-32* and in this paper.

26 – Figure captions should be revised :

“For example : Figure 3, the authors should explicitly mention calculated/simulated electric potential and calculated electric field strength. Figure 9-10, the x axis as labelled 10 20 30 is not appropriate.”

Corrected.

27 – References :

“Ref5 : misspelling of F. Recchia
Ref6 : to be replaced by the suggested one (see above)
Ref7 and 8 : to be merged in a single reference”

Corrected.

.tex file
Click here to download LaTeX Source Files: SIGMA_Modelling.tex

.bib file
Click here to download LaTeX Source Files: SIG_Mod.bib